Pseudo-online detection and classification for upper-limb movements

Journal of Neural Engineering

PAPER

Pseudo-online detection and classification for upper-limb movements

Jiansheng Niu[3] and Ning Jiang[1,2,*]

[1] National Clinical Research Center for Geriatric, West China Hospital Sichuan University, Chengdu, Sichuan, People's Republic of China
[2] Med-X Center for Manufacturing, Sichuan University, Chengdu, Sichuan, People's Republic of China
[3] Department of Systems Design Engineering, University of Waterloo, Waterloo, Ontario, Canada
[*] Author to whom any correspondence should be addressed.

E-mail: jiangning21@wchscu.cn

Keywords: brain-computer interface, electroencephalogram (EEG), upper-limb movement, detection, classification, motor intention

OPEN ACCESS

RECEIVED
2 January 2022

REVISED
4 April 2022

ACCEPTED FOR PUBLICATION
10 June 2022

PUBLISHED
23 June 2022

Abstract

Objective. This study analyzed detection (movement vs. non-movement) and classification (different types of movements) to decode upper-limb movement volitions in a pseudo-online fashion. *Approach*. Nine healthy subjects executed four self-initiated movements: left wrist extension, right wrist extension, left index finger extension, and right index finger extension. For detection, we investigated the performance of three individual classifiers (support vector machine (SVM), EEGNET, and Riemannian geometry featured SVM) on three frequency bands (0.05–5 Hz, 5–40 Hz, 0.05–40 Hz). The best frequency band and the best classifier combinations were constructed to realize an ensemble processing pipeline using majority voting. For classification, we used adaptive boosted Riemannian geometry model to differentiate contra-lateral and ipsilateral movements. *Main results*. The ensemble model achieved 79.6 $\pm$ 8.8% true positive rate and 3.1 $\pm$ 1.2 false positives per minute with 75.3 $\pm$ 112.6 ms latency on a pseudo-online detection task. The following classification gave around 67% accuracy to differentiate contralateral movements. *Significance*. The newly proposed ensemble method and pseudo-online testing procedure could provide a robust brain-computer interface design for movement decoding.

1. Introduction

Brain-computer interface (BCI) based on covert and overt sensorimotor volitions can be used to decode movement intentions from brain activities without external stimuli. Such BCIs are also called endogenous BCIs, which are different from exogenous BCIs dependent on external stimuli, such as those based on P-300 and steady-state-visual evoked potentials (SSVEPs) [1]. Electroencephalogram (EEG) is an electric manifestation of brain activities, recorded non-invasively over the scalp, and it is a main BCI signal source. Endogenous BCIs using EEG have been shown in the literature to have the potential to induce neuroplasticity, making it a potential tool in motor function rehabilitation for stroke survivors and spinal cord injury (SCI) patients [1–6]. As a result, considerable amounts of effort were put into designing a robust BCI system capable of detecting movement intentions [7–9]. In addition to decoding accuracy, which has always been the key performance index in research literature, close-loop delay is a crucial consideration for BCIs targeted at rehabilitation applications, as it is shown to affect the efficiency of neuroplasticity induction [10, 11].

To this end, movement-related cortical potential (MRCP) was explored extensively to decode movement intention due to its short-latency response and natural ballistic movement protocol [12–16]. It is a low-frequency (0.05–5 Hz) EEG generated by movement intentions, starting approximately 1.5–2 s before the movement onset with amplitude between 5 and 30 μV [17]. Apart from MRCP, sensorimotor rhythm (SMR) also gave promising classification results in motor-imagery tasks [18]. However, SMR was normally induced by repetitive executions or imaginations of a movement, which could result in close-loop detection delay [13, 18]. In fact, the detection delay or latencies were usually not reported in SMR studies, which makes it difficult to infer its feasibility to induce neurological plasticity [19, 20]. Nevertheless, some attempts were still made

to combine MRCP and SMR for better decoding performance [21–23].

Currently in the literature, lower-limb studies focusing on ankle dorsiflexion and gait initiation already demonstrated the feasibility of online detection of both covert and overt movement intention through MRCP [10, 12, 14]. Various upper-limb movements have also been experimented for control and rehabilitation purposes, which can be separated into two categories by movement complexity: simple movements including shoulder abduction, elbow/wrist/finger extension [16, 22, 24], and compound movements such as reaching and multi-limb movements [24–27]. The imagery of compound movement was found to have larger power spectral entropy and higher alpha desynchronization than simple movement [24, 25]. Further, MRCPs during proximal movements were found to have higher amplitude than those of distal movements. A statistically significant difference between these two was found from Cz, depending on the joint involved in the movement [28]. The detection accuracy of distal joint movements such as wrist movements were lower than proximal movements, involving the shoulder and elbow [22]. Hence, distal simple movement detection might be more challenging than proximal compound movements.

Among various movement studies, there are essentially two types of objectives: (a) Detection, referring to identifying movement volition (cover or overt) from the rest or idle state, i.e. Mov vs. non-Mov; (b) Classification, referring to identifying a particular type of movement volition from a set of different types of movement volitions, i.e. Mov vs. Mov [21, 22, 27, 29]. Several successful applications of detection were already reported for single movement [27, 30]. Asynchronous classification implicitly includes both detection and classification procedures. However, the form of detection may be different according to experiment protocol and classifier configurations. For example, some studies considered the rest or idle state as one class of the classification task [31, 32], while others split detection and classification into two steps [33, 34].

Both detection and classification need properly designed machine learning models to learn intrinsic signal patterns or features for each class. BCI-related machine learning methods evolved from traditional feature engineering-based approaches to end-to-end deep learning models. Linear discriminant analysis (LDA), a representative traditional method, has been widely applied in MRCP research due to its robust performance. Many studies employed LDA with a shrinkage regularization to achieve state-of-the-art accuracy [30, 31, 33]. Riemannian geometry-based approach is another method between the traditional feature-based method and the deep learning approach. It implicitly embeds temporal and spatial information of EEG into covariance matrices. It was shown to be superior to traditional methods in multiple BCI paradigms, especially for motor imagery [35–37]. More recently, several deep learning architectures were also proposed and showed their potential for BCI applications [38–41]. However, few studies combined these methods to investigate if a further performance boost could be achieved.

In the current study, we investigated the possibility to decode distal simple movements, by analyzing EEG from nine subjects performing four movements: (a) left wrist extension (WE_L), (b) right wrist extension (WE_R), (c) left index finger extension (IE_L), (d) right index finger extension (IE_R). We adopted a hierarchical processing pipeline, where a detection step followed by a classification step. The data analysis was performed in a pseudo-online fashion. Three frequency bands of EEG were investigated for both detection and classification, including low-band (0.05–5 Hz), high-band (5–40 Hz), and full-band (0.05–40 Hz). In the detection step, three classifiers were trained, including an SVM, a Riemannian geometry method, and a deep learning method. Their results were then integrated by majority voting. In the classification step, an adaptive boosted logistic regression model with Riemannian geometry was employed.

2. Method

2.1. Experimental procedure

A total of nine healthy right-handed participants (two F and seven M) were recruited in this study. Ethics approval was granted by the University of Waterloo (approval number 43069). An informed consent form with details of the experimental procedure, experiment equipment, and potential risks was signed by each participant.

The participant was seated in a chair with both forearms placed on a desk. A computer monitor was placed 0.5 m in front of him/her. The participant was required to perform the four movements ballistically during the experiment: WE_L, WE_R, IE_L, and IE_R. Forty-five trials were collected for each movement to yield 180 trials in total. All trials were randomly shuffled, and short breaks were given after 30 consecutive trials. Each participant performed six runs of 30 trails. EEG data were acquired continuously for each run, making it possible to perform pseudo-online analysis. The experimental protocol is schematically shown in figure 1.

In each trial, six visual cues were displayed in the following order in figure 1: Idle, Focus, Prepare, Two, One, and Task. The Focus cue would last for 2 s, followed by the Prepare, Two, and One cue, each of which would last for 1 s. Finally, the Task cue would last for 5 s. The period of one trial was randomized between 13 s and 19 s by varying the Idle time from 3 s to 9 s. The participants were required to perform self-initiating movements at 1 s after Task

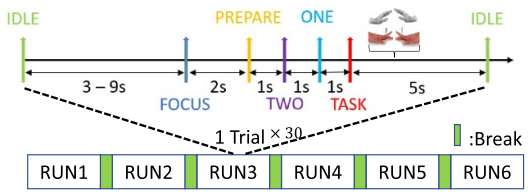

Figure 1. A schematic diagram of the experimental protocol.

cues showed up. A computer voice of the task name was played at the start of each trial. An illustration image and the name of the current task were shown on the screen for each trial.

2.2. Signal acquisition and pre-processing

A multi-channel EEG system (Enobio32, NeuroElectric) was used to collect EEG and electromyography (EMG) data according to the international 10–20 system. EEG data were recorded from 27 channels (Fp1, Fp2, F7, F3, Fz, F4, F8, FC5, FC1, FC2, FC6, T7, C3, C1, Cz, C2, C4, T8, CP5, CP1, CP2, CP6, P7, P3, Pz, P4, P8) at a sampling rate of 500 Hz. The reference electrode was placed at the right earlobe. In addition, four EMG electrodes were attached to the extensor digitorum muscle and the extensor carpi ulnaris muscle on both arms with common reference at the right earlobe to measure muscular activities from index finger extensions and wrist extensions.

EMG signals were firstly filtered by a 6th order non-causal Butterworth bandpass filter with cutoff frequencies of 70 Hz and 200 Hz to remove ECG inference and the power line noise [42]. Then, we applied Teager–Kaiser energy operator (TKEO) to enhance the signal-to-noise ratio [43]. The output of the TKEO operator was further smoothed by a moving averaging to remove short bursts unrelated to the movements. Finally, a threshold of 1/10 of maximum EMG amplitude was applied to extract movement onset.

EEG data were filtered by 4th order non-causal Butterworth bandpass filters to generate three bands of data: low-band (0.05–5 Hz), high-band (5–40 Hz), full-band (0.05–40 Hz). Independent component analysis was applied to decompose the EEG into latent sources. Then, an expert visually inspected the obtained sources and identified those related to eye movements. Finally, the eye-movement-related sources were rejected, and the remaining sources were projected back to sensor space, to reconstruct the EEG. After the data were downsampled to 100 Hz, they were segmented into Mov and non-Mov windows with length of 2 s. The details of segmentation are provided in section 2.8.1. Finally, an expert inspected windows and removed approximately 10% noise-contaminated ones for each subject.

To analyze the brain oscillations, we used Morlet wavelet with five cycles to compute the time-frequency representation with 1 Hz frequency resolution [44, 45]. Then, averaging the power between 5 and 40 Hz from the time-frequency representation gave the high band power, which is illustrated in topographical map. The event-related desynchronization/synchronization (ERD/ERS) from −2 s to 4 s were calculated by subtracting and dividing the mean power during the baseline (−3 s to −2 s) [46]. EEG preprocessing and brain oscillation analyses were performed by Python MNE package [47].

2.3. Riemannian geometry

On the Riemannian manifold, each point stands for a symmetric positive definite matrix, we need to transfer EEG data into this form to utilize the properties of Riemannian geometry. An event-related potential (ERP) covariance matrix was constructed for this purpose to capture both temporal and spatial information [35]. For detection task, each window was firstly stacked with Mov template (average of all Mov windows) and non-Mov template (average of all non-Mov windows) to construct a super window, which was in shape of $(27 \times 3, 200)$. Then, an ERP covariance matrix was obtained by multiplying the super window with its transpose, which was in shape of $(27 \times 3, 27 \times 3)$ [35]. For WE-vs.-IE classification, each window was stacked with WE template (average of all WE windows) and IE template (average of all IE windows) to build the super window and the following ERP covariance matrix. Similar procedure was repeated for left-vs.-right classification. As a result, the classification ERP covariance matrix was also in shape of $(27 \times 3, 27 \times 3)$.

Then, every point was projected to a tangent space by logarithmic mapping to form a feature vector as the input to classical algorithms. The feature vector was in dimension of $n \times (n + 1)/2$, where n was the row or column size (27×3) of the ERP covariance matrix [48]. This study constructed two classifiers on tangent space: SVM and adaptive boosted (Ada-boost) logistic regression, called R_SVM and R_Ada_Lgr, respectively.

2.4. EEGNET

Another algorithm we used was EEGNET, a compact deep learning architecture designed specifically for decoding EEG and was successfully applied in multiple paradigms [38]. It utilized three convolutional layers to extract temporal and spatial information from data. The input to this model was a 2D matrix with dimensions of channel and sample, in shape of (27, 200) as 2 s window was used. The first layer added a convolutional kernel with size (1, 50) to filter each channel in temporal order. The output of the first layer contained temporally filtered data. The second layer applied a (27, 1) kernel (27 being the channel number) on the output of the first layer to assign a weight to each channel and embedded spatial information in its output. A separable conv2d layer

integrated temporal and spatial information learned from the first and second layers. Finally, the classification was made after a fully connected layer using SoftMax. Its optimizer was Adam, and its loss function was categorical cross-entropy. We fine-tuned the number of filters used in each layer (F1 = 8, D = 6, F2 = 48) [38]. The optimal drop rate was set to 0.5.

2.5. SVM

SVM has been widely applied in the BCI field. It finds the largest margin between classes by solving an optimization problem based on sample vectors. EEG data were transformed to 1D by concatenating the samples of all channels, resulting in a 5400 (27×200) long feature vector for a 2 s window. Then, the 1D feature vector was provided to a SVM with radial basis function kernel as its input, to learn the intrinsic features of each class.

2.6. Detection fusion

The detection results of EEGNET, R_SVM, and SVM were post-processed by a simple ensemble method. First, these three classifiers individually predicted each window as Mov or non-Mov. Then the final label for the window was assigned using majority voting.

2.7. Classification method

AdaBoost was used for the Classification task. AdaBoost is another ensemble learning method that sequentially trains a weak learner (classifiers with slightly above chance-level performance) on continuously re-weighted samples to boost its performance. Logistic regression was chosen to be the weak learner in this study. AdaBoost trained ten logistic regression models using Riemannian features for classification.

2.8. Pseudo-online analysis

In an online BCI scenario, the algorithm analyzes real-time data and constantly makes predictions. In order to simulate the online scenario after the data collection, we used the sliding window technique to process the continuously acquired EEG data, i.e. in a pseudo-online way. In this analysis, the detection classifiers firstly predicted a window as Mov or non-Mov. Then, the classification classifier further predicted the movement type of the Mov windows.

We conducted six-fold cross-validation based on six runs to evaluate the classifier performance. Allocation of training, testing, and validation runs were different for different algorithms. For example, EEGNET used four runs for training, one run for validation, and the remaining one run for testing. However, R_SVM, SVM and R_Ada_Lgr utilized five runs for training and the remaining one run for testing, as no hyperparameter tuning was necessary.

In order to analyze the impact of EEG frequency bands on classifiers, the detection and classification algorithms were trained using three frequency bands data (low, high, and full). Training and testing of one algorithm used the same frequency band.

2.8.1. Pseudo-online detection

In the training phase, we firstly separated Mov and non-Mov segments in the training trials. As shown in figure 2, Mov segment spans from −1.6 s to 0.6 s of each trial, while non-Mov segment contains two segments: from −8 s to −2 s and from 2 s to 8 s, with 0 s being the movement onset (identified by the EMG processing). Then, Mov and non-Mov segments were scanned by a 2 s time window with 0.01 s stride and 0.05 s stride, respectively, to generate multiple windows. The longer stride was chosen for non-Mov segments to save computational power. In order to balance the Mov and non-Mov windows, 21 windows were randomly selected from 162 non-Mov windows to match the amount of Mov windows in each trial.

In the testing phase, the testing run was scanned by a 2 s time window with 0.1 s stride to obtain testing windows, as shown in figure 2. As described in section 2.6, these windows were firstly classified by EEGNET, R_SVM, and SVM individually. Then, the final predictions were obtained by the ensemble method through majority voting. Unanimous voting of multiple consecutive windows was investigated as well.

Four performance metrics were introduced for evaluation: true positive rate (TPR), false positives per minute (FPs min^{-1}), F1 score, detection latency. TPR was the number of TPs (green points in figure 2) divided by the sum of TPs and FNs (blue points in figure 2). FPs min^{-1} was the number of FPs (red points in figure 2) divided by the duration of non-Mov state. TPR and FPs min^{-1} were presented in a receiver operator characteristic (ROC) curve by varying the number of consecutive windows used for unanimous voting. A 2 s refractory time was applied to prevent classifiers from generating new detections within 2 s of the last one. Since some classifiers were trained on low-band MRCP whose length is 2 s, it was not reasonable to make multiple detections for one intention. F1 score represented the trade-off between precision and recall, which was computed by $\text{TP}/(\text{TP} + 0.5 \times (\text{FP} + \text{FN}))$. As Mov period was shorter than non-Mov period, F1 score was chosen due to its robustness in imbalanced scenarios [39]. Detection latency was defined as the time difference between movement onset and detected onset.

2.8.2. Pseudo-online classification

Following the detection, the classification of four movements was performed by R_Ada_Lgr. The training windows were extracted by a 2 s time window with 0.01 s stride on Mov segments (i.e. −1.6 s–0.6 s of the trials) for each trial. We investigated left-vs.-right and WE-vs.-IE classifications by combining their training windows accordingly. For example, left-vs.-right classification combined windows of WE_L and IE_L as

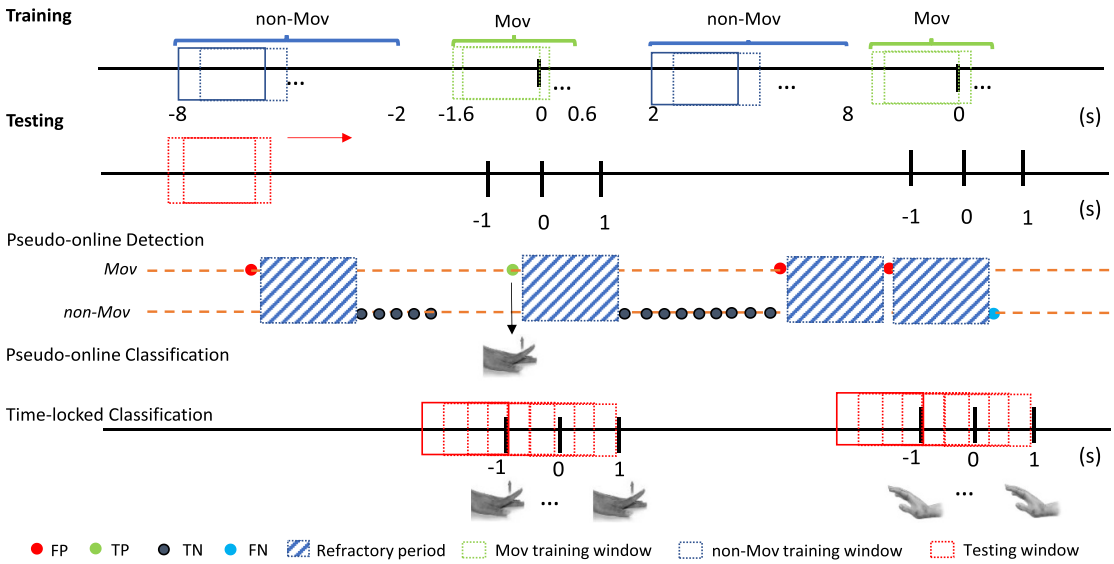

Figure 2. Schematic diagram of the training and testing procedures for pseudo-online and time-locked analysis. A random recording portion consisting of two trials is illustrated in timelines to demonstrate the details of training and testing in pseudo-online and time-locked analyses. Training of both analyses were identical, shown in the top timeline. A 2 s window (green rectangle) scanned each trial between −1.6 s and 0.6 s with a stride of 0.01 s, giving 21 Mov training windows in total. Likewise, a 2 s window (blue rectangle) scanned each trial from −8 s to −2 s and from 2 s to 8 s with a stride of 0.05 s, generating 162 non-Mov windows in total. During testing, a 2 s window (red rectangle) moves with a stride of 0.1 s through the entire testing run. In pseudo-online detection, each testing window was first predicted as either Mov or non-Mov, shown as points on the two orange dashed lines. The valid period for detection was between −1 s and 1 s of each trial. Windows predicted as Mov in this period were TPs (green point). In the contrary, those predicted as non-Mov in this period were FNs (blue point). Outside of this period, windows predicted as Mov were FPs (red point), and those predicted as non-Mov were TNs (gray point). A refractory period (blue strip rectangle) paused detection for 2 s after a Mov prediction. Only TP windows were further classified to a movement type. In time-locked classification, a 2 s window scanned within −1 s–1 s of each trial with a stride of 0.1 s, giving 21 windows.

the Left class and windows of WE_R and IE_R as the Right class. The similar procedure was conducted for WE-vs.-IE classification as well.

During testing, the current time window would be predicted by the trained R_Ada_Lgr once a detection was triggered, as shown in figure 2. The accuracy and confusion matrix evaluated the classification performance on trial-level as one trial gave one classification label.

2.9. Time-locked classification

Time-locked classification was performed to analyze the performance of classification using the three bands. It generates predictions for all windows between −1 s and 1 s of each trial, as shown in figure 2, in contrast to classifying only the detected window in the pseudo-online scenario.

We investigated WE-vs.-IE and Left-vs.-right classification in time-locked fashion as well. The training set window extraction was the same as the pseudo-online classification. The testing was conducted on all windows of testing trials as shown in figure 2. The accuracy of every window was computed in a trial-based manner, meaning that the proportion of correctly classified trials was the accuracy for that window.

2.10. Statistical analysis

We conducted two-way analysis of variance (ANOVA) to investigate the effect of ten models on movement detection. The fixed factor was the detection model with ten levels: ensemble model and three sub-models trained by three frequency bands, as shown in figure 3. The subject was considered as a random factor. The null hypothesis was the detection models did not have significant influence on the performance index, i.e. the F1 score. Upon detecting a statistical significance, we performed Bonferroni pairwise comparison with 95% confidence interval. Ten models were grouped based on their difference of mean [49]. Groupings were indicated by letters, those not sharing the same letter were significantly different.

The same approach was conducted to test if frequency band played a significant role during pseudo-online classification. Two-way ANOVA was performed by choosing frequency bands as fixed factor and subject as random factor. The Bonferroni pairwise comparison with 95% confidence interval generated grouping information. All statistical analyses were performed using Minitab Ver. 21.

3. Results

3.1. Pseudo-online detection and classification

To evaluate the performance of multiple classifiers in different frequency bands, figure 3 presents the violin plots of F1 scores for ten combinations between different algorithms and frequency bands. There were 54 F1 scores computed for each combination (nine subjects, each with six runs). The ANOVA test showed

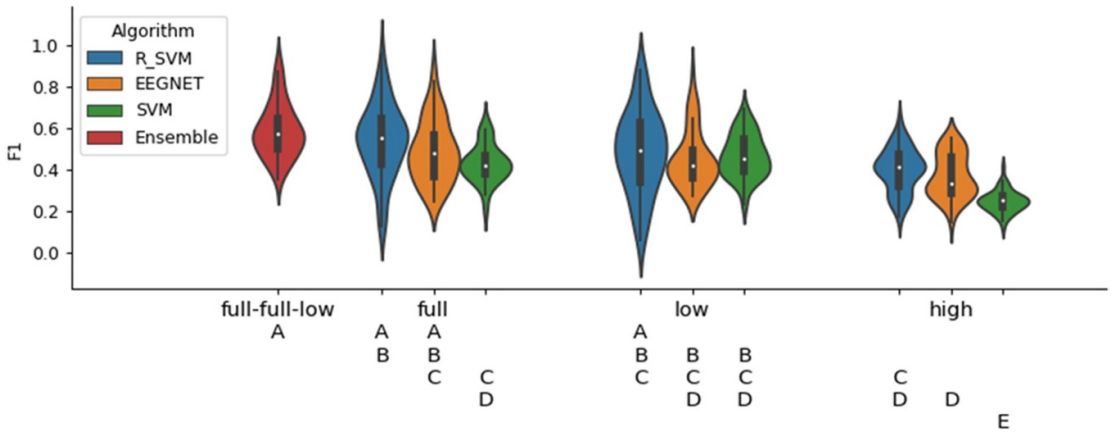

Figure 3. Violin plots of F1 scores for all classifiers using different bands. Four algorithms including R_SVM, EEGNET, SVM and ensemble method are presented as blue, yellow, green and red, respectively. Results of full, low, and high frequency bands are clustered in three groups. The ensemble method consists of full-band trained R_SVM, full-band trained EEGNET and low-band trained SVM, which is shown as full-full-low. For each violin plot, the median value is shown as the white point, the black bar represents the interquartile range, the line out of bar represents the rest of the distribution. The outer curve is the kernel density of the data distribution. The letters below the plot show the significant groups calculated by Bonferroni pairwise comparison with 95% confidence interval. Groups that do not share a letter are significantly different.

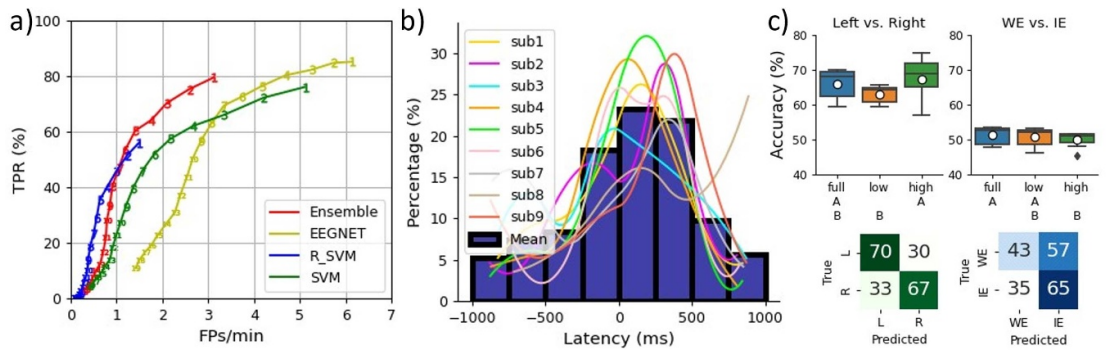

Figure 4. Results of pseudo-online detection and classification. Panel (A) shows the detection ROC of ensemble method, SVM, R_SVM and EEGNET in red, green, blue, and yellow, respectively. Points in each line are represented by the numbers. They stand for the number of consecutive time windows needed to trigger detection, starting from 1 on the right-upside to 19 on the left-downside. Panel (B) demonstrates the percentage histogram of detection latencies using ensemble method for every subject (color curves) and mean of all subjects (purple bars in the foreground). Panel (C) shows the accuracy boxplots and the confusion matrices of left-vs.-right and WE-vs.-IE classifications. For each boxplot, full, low and high band accuracies are shown in blue, yellow and green, respectively. The mean accuracy of nine subejcts are shown as white point. The letter below each band shows the significance grouping calculated by Bonferroni pairwise comparison with confidence level of 95%. Groups that do not share a letter are significantly different. The green confusion matrix represents the high-band classification result for left-vs.-right, while the blue confusion matrix represents the full-band classification result for WE-vs.-IE. They are normalized so that the sum of each row is 100.

that detection model had a significant effect on F1 score (degree of freedom = 9, $F = 17.11$, $p < 0.001$). Further Bonferroni pairwise comparison showed that full-band trained classifiers were significantly better than low-band trained classifiers since they did not share same grouping letter, as shown in figure 3. Three algorithms showed their adaptation for different frequency bands. For instance, R_SVM and EEGNET performed best using the full-band, while SVM got the highest F1 scores with the low-band. As a result, the ensemble method was constituted by full-band trained R_SVM and EEGNET along with low-band trained SVM, shown as the red violin plot in figure 3. Overall, the ensemble method achieved the highest F1 score and was significantly better than most of the sub-models including full-band trained SVM, low-band trained EEGNET, low-band trained SVM and all high-band trained models based on significant groupings shown in figure 3.

From these results, subsequent analyses adopted full-band trained EEGNET, full-band trained R_SVM, low-band trained SVM, and the ensemble method without mentioning the band explicitly.

To assess the performance of pseudo-online processing, detection ROC curve, detection latency histogram and classification accuracy with confusion matrix are shown in figure 4. In figure 4(a), TPR and FPs min^{-1} for different classifiers are presented as points on ROC curves with the number of consecutive windows required to trigger detections as

Table 1. Pseudo-online detection TPR, FPs min^{-1} and latencies using the ensemble method.

Subject	TPR %	FPs (min)	Latencies (ms)
1	85.5	3.3	32.0
2	84.8	3.4	62.7
3	75.2	4.4	7.2
4	85.0	3.0	16.8
5	96.0	1.8	64.5
6	77.3	2.8	121
7	68.2	4.2	−61.2
8	73.4	0.9	340.1
9	71.2	4.3	94.6
Mean ± SD	79.6 ± 8.8	3.1 ± 1.2	75.3 ± 112.6

the threshold. ROC was chosen to show the impact of consecutive detection window number on classifier performance. For all algorithms, with the required number of consecutive windows increasing, TPR and FPs min^{-1} decreased, graphically moving from the upper right side to the lower left side along the respective ROC curve. Compared to the ensemble method with the same window number, EEGNET produced both higher TPs and FPs min^{-1}, while R_SVM provided a lower FPs min^{-1}, but at the cost of lower TPR. SVM's performance was more balanced between EEGNET and R_SVM. As a result, the ensemble method performed better than the three individual classifiers, with both lower FPs min^{-1} and higher TPR (the red line located on the left-upper side of others in the ROC plot (figure 4(a)). One window was adopted for detection in the subsequent analysis since it provided the best TPR with reasonable FPs min^{-1}.

Detection latency is the time difference between the detection and its corresponding movement onset identified by EMG processing. Histograms were obtained by counting the percentage of correct detections fallen into eight subsections of 250 ms width from −1000 ms to 1000 ms, as shown in figure 4(b). Detection latency was shown for each subject and the mean of them. Direct observation indicates that the average latency of all subjects was between 0 and 250 ms. In addition, approximately 70% of detections happened within ±500 ms of the movement onset. Moreover, most subjects' latency distributions (with one exception of subject 8) were similar to the mean histogram, indicating consistency across the subject pool.

Table 1 summarizes all subjects' TPR, FPs min^{-1}, and latencies. It shows the mean and standard deviation among subjects. Subject 5 gave the best TPR as 96.0%, and subject 8 gave the best FPs min^{-1} as 0.9. The shortest latency was achieved by subject 7, which is −61.2 ms. The mean latency across all subjects is 75.3 ±112.6 ms.

The pseudo-online classification results are presented in figure 4(c). For classification between left and right movements, the ANOVA test showed frequency band had a significant effect on classification accuracy (degree of freedom = 2, $F = 6.41$, $p = 0.009$). The accuracy plot shows that the high-band trained R_Ada_Lgr performed best in terms of the mean accuracy among subjects. Besides, it is significantly better than the low-band trained model according to their statistical grouping. The normalized classification confusion matrix representing the high-band trained R_Ada_Lgr indicates that 70% of the left and 67% of the right movements were correctly classified. For classification between WE and IE, the ANOVA test also indicated that frequency band had a significant effect on accuracy (degree of freedom = 2, $F = 6.98$, $p = 0.007$). The accuracy of the full-band trained R_Ada_Lgr was significantly better than the high-band one in terms of their statistical grouping. The normalized confusion matrix further illustrates the full-band accuracy, showing that 43% of WE and 65% of IE were correctly classified. Observing boxplots and confusion matrix in figure 4(c) shows that the overall accuracy of WE-vs.-IE classification is worse than left-vs.-right classification.

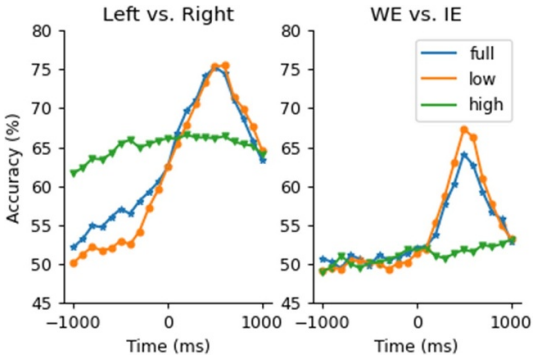

Figure 5. Time-locked classification results. Time-locked classification accuracy of left-vs.-right and WE-vs.-IE are shown in the left and right graphs, respectively. Each graph shows 21 accuracies measured from −1000 ms to 1000 ms with 100 ms interval. Full, low and high band result are shown in blue, yellow and green, respectively. Each line is the mean accuracy of nine subjects.

3.2. Time-locked classification

The classifications of WE-vs.-IE and left-vs.-right were also investigated in time-locked manner using full, low and high bands, as shown in figure 5. The accuracies of low-band and full-band show time-locking effect in both classifications. The accuracy curves reach their peaks at approximately 500 ms and then drop down. In contrast, the high-band accuracy does not have strong relationship with time. In left-vs.-right classification, the full- and low-band accuracies start at around 50% at −1000 ms and achieve similar peaks of approximately 75% at 500 ms. Then they both decrease to around 64% at 1000 ms. However, the high-band accuracy slowly increases from approximately 62% at −1000 ms to

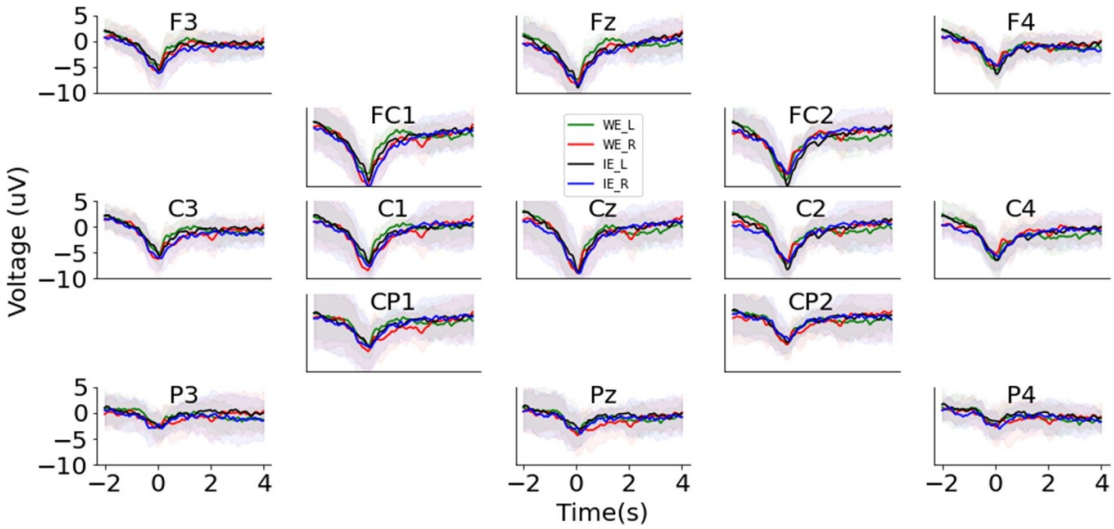

Figure 6. MRCP morphologies across motor cortex. Grand averages of MRCPs for four movements including WE_L, WE_R, IE_L and IE_R are drawn in green, red, black and blue colors, respectively. In each plot, time ranges from −2 s to 4 s and voltage ranges from −10 to 5 μV. The inter-subject standard deviation is shown as shaded colors behind the average MRCPs.

around 66% at 200 ms and keeps steady afterwards. In WE-vs.-IE classification, the low and full band accuracies increase from around 50% at −1000 ms and reach peaks to 67% and 64% at 500 ms, respectively. Then, they both drop down to approximately 53%. Nevertheless, the high-band accuracy fluctuates at around 51% between −1000 ms and 1000 ms.

In addition, all three bands show that the left-vs.-right movements are classified easier than the WE-vs.-IE classification on the same limb by observing figure 5.

3.3. MRCP

Grand averages of MRCP were calculated by averaging the mean MRCPs for each subject. From figure 6, we can see MRCPs are diffusely identifiable over the motor cortex with similar morphology: sharply decreasing Bereitschaftspotential from −2 s to 0 s, followed by a quick rebounding phase from 0 s to 1 s. Specifically, frontal, frontal-central, and central channels showed larger MRCP amplitudes than other central-parietal and parietal channels. The maximal peak-to-peak MRCP amplitude is approximately 12 μV in FC1, FC2, and Cz. Slight lateralization can be seen on FC1, FC2, C1, and C2. For example, the negative peak amplitude of WE_L is larger than WE_R on FC2 but smaller than WE_R on FC1. The same pattern is found for IE as well, the negative peak amplitude of IE_L is larger than IE_R on FC2 and C2, while it is slightly smaller than IE_R on FC1 and C1. However, the morphology difference between WE and IE of same side are not found in figure 6.

3.4. ERD/ERS

High band ERD/ERS were calculated for four classes by averaging all trials in nine subjects and shown in figure 7. By observing topographical maps, ERD starts from −1 s and shows slight lateralization on WE_L and IE_L over FC2, C2 and C4. Then ERS emerges from 3 s and distributes contralaterally. However, the lateralization is not localized to specific channels for ERS. The detailed ERD/ERS for C1 and C2 are shown in the right plot of figure 7. The ERDs of C1 and C2 decrease from 0 at −2 s to around −30% at around 0 s and start rebounding afterwards. The ERS appears at around 3 s and increases to approximately 10% at 4 s. The ERD difference between C1 and C2 is observable but subtle. However, the ERS difference could be found between 3 s and 4 s. The ERS of C2 is higher than C1 in WE_L and IE_L tasks, while lower than C1 in WE_R and IE_R tasks. Overall, the time-locking effect of ERD/ERS is less prominent than MRCP. Similar to MRCP, the ERD/ERS do not give observable difference between WE and IE tasks on the same limb either.

4. Discussion

4.1. Algorithm and frequency band

The current study investigated the performance of three detection algorithms (R_SVM, EEGNET, and SVM) and one classification algorithm (R_Ada_Lgr) on three different frequency bands (low, high, and full) in the context of identifying four different motor volitions from EEG signals.

In detection, differences among frequency bands were found in nearly all classifiers. According to figure 3, the F1 score of the full-band is significantly better than the high-band for all classifiers. Besides, the low band is also generally better than the high band though not all classifiers showed significant differences. MRCP and ERD/ERS morphology could explain this preference on the full- and low-band over

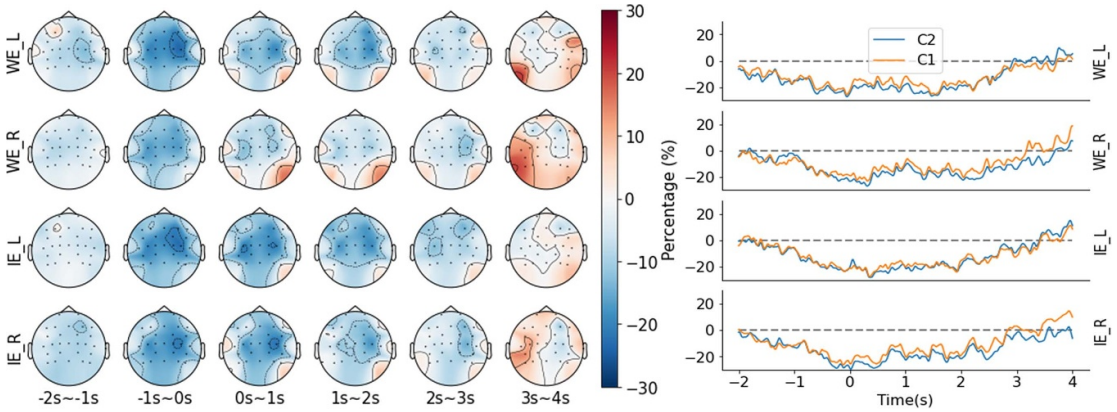

Figure 7. High band ERD/ERS. High band (5–40 Hz) ERD/ERS are drawn for four classes from −2 s to 4 s with respective to baseline period (−3 s to −2 s). The left plot shows the power change in topographical maps, the color bar shows the percentage change from −30% to 30%. The right plots show ERD/ERS of C1 and C2 in orange and blue, respectively. The dashed line is zero percentage change line. ERS is the portion above the line, while ERD is the portion below the line.

the high-band. Evidently from figures 6 and 7, MRCP has a clear negative peak, which is time-locked to movement onset. This time-lock feature of MRCP is more pronounced than any feature of ERD/ERS. It can be inferred that MRCP contains critical discriminant information in ballistic movement detection when consistency in detection latency is required, such as in applications focusing on neural plasticity induction.

In pseudo-online classification, frequency bands also showed an impact on performance. Figure 4(c) showed that the high-band performed significantly better than the low-band when classifying between left and right movements, suggesting the valuable information for lateral classification exists in ERD/ERS. This is supported by the contra-lateral activation of ERD/ERS shown on topographical maps (figure 7). However, the classification between WE and IE presented a different scenario. The full-band provided the best performance and was significantly better than the high-band, as shown in figure 4(c). Since neither the MRCP nor ERD/ERS showed a noticeable difference between WE and IE, the full-band might integrate useful information from the other two bands.

The analyses of different frequency bands revealed different time-related classification behaviors as well. As shown in figure 5, the high-band accuracy was not sensitive to time in both classification tasks, while the full- and low- band had a clear time-locking effect. This could be explained by more abrupt morphology change in MRCP than ERD/ERS between −1 s and 1 s by observing figures 6 and 7.

Classifiers had their preferences over frequency bands. For example, R_SVM and EEGNET achieved the highest F1 score with full-band data, while SVM performed best with low-band data. It was not surprising that EEGNET performed well on the full band since it resembles the properties of filter bank common spatial pattern algorithm, which requires wide frequency bandwidth to generate various temporal features [38]. Riemannian geometry-based method also proved their efficacy on various frequency bands of EEG such as 8–30 Hz for motor imagery, 1–16 Hz for ERP, and individual frequencies for SSVEP [35, 50–52]. However, to the authors' best knowledge, full-band EEG was never used with the Riemannian geometry method. The better performance of Riemannian geometry method in the full band over the other two bands might provide a new angle for this algorithm in the context of sensorimotor EEG decoding. SVM preferred low-band EEG, which is in line with various MRCP studies in the literature that achieved state-of-art results using SVM [53, 54].

The ensemble method was constructed by majority voting of the three classifiers. After individual frequency band tests on algorithms, full-band EEGNET, low-band SVM, and full-band R_SVM were selected to be sub-models for the ensemble classifier. As a result, this classifier showed significantly better results on F1 scores than six algorithms as mentioned in section 3.1. Besides, its ROC curve was also better than three sub-models trained on their best bands, as shown in figure 4(a).

4.2. Detection

Pseudo-online analysis was widely used in the BCI field to simulate the real-time EEG processing, particularly in analyses of various pipeline hyperparameters, which are impractical to perform fully online [13, 14, 27, 32, 55, 56]. It is a more realistic approach than the traditional epoch-based offline processing because the data were treated as time windows coming through classifiers as if they were processed online. Further development in online studies would benefit from the experiences acquired in pseudo-online analysis. Among these studies, there were some discrepancies in how the testing data should be constructed. For example, some studies tested on individual trials, the robustness of these pseudo-online

analyses will be limited if the testing trials are pre-selected short portions that might not represent the actual rest state [27, 34]. To resemble the real-time scenario more closely, our testing data used entire continuous recordings of experimental runs of approximately 10 min duration, and no manual selections of trials were conducted in the testing run.

The pseudo-online of the current study showed four movements were successfully detected with average TPR as 79.6% ± 8.8% and average FPs min^{-1} as 3.1 ± 1.2. A fair amount of pseudo-online studies chose the TPR and FPs min^{-1} as performance metrics [14, 55, 56]. One study investigated pedaling volition and achieved 76.7% TPR with 4.94 FPs min^{-1} on five healthy subjects [55]. Another paper reported 68.67% TPR and 18.09 FPs min^{-1} on gait intention investigation when pre-set specificity is 70% [56]. Although most of the studies are still in offline or pseudo-online stages, one demonstrated the possibility of detecting upper-limb movements in real-time on one SCI patient [33]. Shrinkage LDA was used to detect and classify MRCP for two movements (hand open and palmar grasp) in real-time. In the best session, the detection performance gave 36.9% TPR and 3.6 FPs min^{-1}. The low TPR in this study might be affected by the small sample number, non-healthy participants, and challenges in online system design [33]. A following study investigated the reach-and-grasp detection on 20 non-disabled participants in online scenario by taking gaze shifting into consideration [57]. They proposed a hierarchical classification to first detect movement from rest and then differentiate movement from looking. The online evaluation achieved TPR of 54% and 1.7 FPs min^{-1} on rest. Their TPR was lower than ours but had a better FPs min^{-1}. However, a direct comparison is hard due to different experimental protocol.

Detection latency is a crucial factor for rehabilitation-aimed BCI devices since Hebbian plasticity could only be induced within a short close-loop delay [11]. In the BCI context, volition detection from the EEG algorithm should occur within 400–500 ms of the volition onset. Otherwise, the causal relationship between volition and afferents feedback generated by the BCI would be compromised [10]. In this study, the average latency was 75.3 ± 112.6 ms, which is in this range. Short-latency BCIs mostly rely on the MRCP features in the movement decoding field, while few SMR studies mentioned their latencies [12–14, 19, 20]. In this current study, both full-band and low-band EEG contributed to the detection and obtained short-latency performance, suggesting full-band EEG has the potential for short-latency BCI design when it includes MRCP.

Latencies were normally examined by inter-subject average and standard deviation [10, 12–14, 27]. Nevertheless, the intra-subject latency variability was largely overlooked. In a real rehabilitation application, only those detections made within the optimal plasticity inducement period could be considered useful trials. As figure 4(b) shows, around 70% of trials were detected between −500 ms and 500 ms, although the group level latency is 75.3 ± 112.6 ms. Future studies should consider this to test the efficacy of the system.

4.3. Classification

Two types of classification, including left-vs.-right and WE-vs.-IE, were investigated in pseudo-online and time-locked manners. In general, we can find left-vs.-right classification had better performance than WE-vs.-IE classification across all bands in both manners, as shown in figures 4(c) and 5. This is in line with the MRCP and ERD/ERS findings, which show subtle difference in contra-lateral movements but no difference between ipsilateral movements.

From the time-locked classification analysis in figure 5, we can find a clear accuracy peak at around 500 ms after movement onset for low- and full-band EEG. This indicated the most differentiable information of these two bands located in −1.5 s to 0.5 s with respective to onset, which is consistent with the period of MRCP. However, the accuracy of the high-band does not show time-sensitive change, which is in line with the smooth ERD/ERS shape on the right plot of figure 7.

Pseudo-online classification was done on detected windows. Since the time-locking effects exist in the low- and full-bands, it is important to note that the detection latency could significantly affect the subsequent classification performance. For example, a trial detected on 500 ms after movement onset would have the best chance to be correctly classified by the low- and full-band because their accuracies were the highest approximately 500 ms, as shown in figure 5. However, the detection latency distribution from figure 4(b) shows a large variability between −1000 ms and 1000 ms, leading to slightly worse classification results on pseudo-online classification. Unlike the low- and full-band, the high-band did not show clear time-locking effect. In left-vs.-right classification, its relative stable accuracy at around 64% on time-locked classification (figure 5) provided the best mean accuracy on pseudo-online classification (see figure 4(c)), leading a significantly more robust overall system performance. In WE-vs.-IE classification, however, the high-band showed constantly low accuracy during the detection period, making it the worst band on pseudo-online classification.

4.4. Study limitations

Although this study provided a state-of-art detection solution in pseudo-online detection, the classifications among ipsilateral movements are far from practical. Future investigations on locking the best classification period after detection might be worth investigating. Another major limitation is that this study still performs a post-experiment offline analysis. The

current study did not fully explore many real-time processing challenges, including filter design, computational latencies, and complexity analysis of the classifiers.

5. Conclusion

This study has demonstrated the feasibility of detecting simple distal upper-limb movements (WE_L, WE_R, IE_L, IE_R) in a pseudo-online scenario. An ensemble learning method was proposed to detect movement intentions using mixed band features. Within nine subjects, the best case shows 96% of the intentions being detected in subject 5, and less than one non-Mov window was misclassified per minute in subject 8. Seven out of nine subjects' movement intentions were predicted within 100 ms latency on average. The following classification step also proves its possibility to differentiate lateral movements with around 67% accuracy using high-band EEG. Further investigation showed there is a time-locking effect on classification on the low- and full-band. The explorations on MRCP and ERD/ERS revealed different EEG patterns of movements and explained the results of detection and classification.

Data availability statement

The data generated and/or analysed during the current study are not publicly available for legal/ethical reasons but are available from the corresponding author on reasonable request.

Acknowledgments

This work was supported by West China Hospital Sichuan University; and Ministry of Research Innovation and Science of Ontario. The authors would like to thank all participants for contributing their time and effort to the experimental part of this study.

ORCID iDs

Jiansheng Niu https://orcid.org/0000-0001-8002-4691
Ning Jiang https://orcid.org/0000-0003-1579-3114

References

[1] Abiri R, Borhani S, Sellers E W, Jiang Y and Zhao X 2019 A comprehensive review of EEG-based brain–computer interface paradigms *J. Neural. Eng.* **16** 011001
[2] Jackson A and Zimmermann J B 2012 Neural interfaces for the brain and spinal cord—restoring motor function *Nat. Rev. Neurol.* **8** 690
[3] Ang K K and Guan C 2013 Brain-computer interface in stroke rehabilitation *J. Comput. Sci. Eng.* **7** 139–46
[4] Cervera M A, Soekadar S R, Ushiba J, Millán J D R, Liu M, Birbaumer N and Garipelli G 2018 Brain-computer interfaces for post-stroke motor rehabilitation: a meta-analysis *Ann. Clin. Transl. Neurol.* **5** 651–63
[5] Langhorne P, Coupar F and Pollock A 2009 Motor recovery after stroke: a systematic review *Lancet Neurol.* **8** 741–54
[6] Dobkin B H 2004 Strategies for stroke rehabilitation *Lancet Neurol.* **3** 528–36
[7] Al-Quraishi M S, Elamvazuthi I, Daud S A, Parasuraman S and Borboni A 2018 EEG-based control for upper and lower limb exoskeletons and prostheses: a systematic review *Sensors* **18** 3342
[8] Hortal E, Planelles D, Resquin F, Climent J M, Azorín J M and Pons J L 2015 Using a brain-machine interface to control a hybrid upper limb exoskeleton during rehabilitation of patients with neurological conditions *J. Neuroeng. Rehabil.* **12** 1–6
[9] Bhagat N A *et al* 2016 Design and optimization of an EEG-based brain machine interface (BMI) to an upper-limb exoskeleton for stroke survivors *Front. Neurosci.* **10** 122
[10] Xu R, Jiang N, Mrachacz-Kersting N, Lin C, Prieto G A, Moreno J C, Pons J L, Dremstrup K and Farina D 2014 A closed-loop brain–computer interface triggering an active ankle–foot orthosis for inducing cortical neural plasticity *IEEE Trans. Biomed. Eng.* **61** 2092–101
[11] Mrachacz-Kersting N, Kristensen S R, Niazi I K and Farina D 2012 Precise temporal association between cortical potentials evoked by motor imagination and afference induces cortical plasticity *J. Physiol.* **590** 1669–82
[12] Xu R, Jiang N, Lin C, Mrachacz-Kersting N, Dremstrup K and Farina D 2013 Enhanced low-latency detection of motor intention from EEG for closed-loop brain-computer interface applications *IEEE Trans. Biomed. Eng.* **61** 288–96
[13] Xu R, Jiang N, Mrachacz-Kersting N, Dremstrup K and Farina D 2016 Factors of influence on the performance of a short-latency non-invasive brain switch: evidence in healthy individuals and implication for motor function rehabilitation *Front. Neurosci.* **9** 527
[14] Niazi I K, Jiang N, Tiberghien O, Nielsen J F, Dremstrup K and Farina D 2011 Detection of movement intention from single-trial movement-related cortical potentials *J. Neural. Eng.* **8** 066009
[15] Ofner P, Schwarz A, Pereira J, Wyss D, Wildburger R and Müller-Putz G R 2019 Attempted arm and hand movements can be decoded from low-frequency EEG from persons with spinal cord injury *Sci. Rep.* **9** 7134
[16] Ofner P, Schwarz A, Pereira J, Müller-Putz G R and Zhang D 2017 Upper limb movements can be decoded from the time-domain of low-frequency EEG *PLoS One* **12** e0182578
[17] Wright D J, Holmes P S and Smith D 2011 Using the movement-related cortical potential to study motor skill learning *J. Mot. Behav.* **43** 193–201
[18] Chu Y, Zhao X, Zou Y, Xu W, Song G, Han J and Zhao Y 2020 Decoding multiclass motor imagery EEG from the same upper limb by combining Riemannian geometry features and partial least squares regression *J. Neural. Eng.* **17** 046029
[19] Schwarz A, Scherer R, Steyrl D, Faller J and Müller-Putz G R 2015 A co-adaptive sensory motor rhythms brain-computer interface based on common spatial patterns and random forest *2015 37th Annual Int. Conf. IEEE Engineering in Medicine and Biology Society (EMBC)* (*25 August 2015*) (IEEE) pp 1049–52
[20] Pfurtscheller G, Brunner C, Schlögl A and Da Silva F H 2006 Mu rhythm (de) synchronization and EEG single-trial classification of different motor imagery tasks *NeuroImage* **31** 153–9
[21] Bai O, Lin P, Vorbach S, Li J, Furlani S and Hallett M 2007 Exploration of computational methods for classification of movement intention during human voluntary movement from single trial EEG *Clin. Neurophysiol.* **118** 2637–55
[22] López-Larraz E, Montesano L, Gil-Agudo Á and Minguez J 2014 Continuous decoding of movement intention of upper limb self-initiated analytic movements from pre-movement EEG correlates *J. Neuroeng. Rehabil.* **11** 1–5

[23] Sburlea A I, Montesano L, de la Cuerda R C, Alguacil Diego I M, Miangolarra-Page J C and Minguez J 2015 Detecting intention to walk in stroke patients from pre-movement EEG correlates *J. Neuroeng. Rehabil.* **12** 1–2
[24] Yi W, Qiu S, Qi H, Zhang L, Wan B and Ming D 2013 EEG feature comparison and classification of simple and compound limb motor imagery *J. Neuroeng. Rehabil.* **10** 1–2
[25] Yi W, Qiu S, Wang K, Qi H, Zhang L, Zhou P, He F, Ming D and Maurits N M 2014 Evaluation of EEG oscillatory patterns and cognitive process during simple and compound limb motor imagery *PLoS One* **9** e114853
[26] Lew E, Chavarriaga R, Silvoni S and Millán J D 2012 Detection of self-paced reaching movement intention from EEG signals *Front. Neuroeng.* **5** 13
[27] Randazzo L, Iturrate I, Chavarriaga R, Leeb R and Millán J D 2015 Detecting intention to grasp during reaching movements from EEG *2015 37th Annual Int. Conf. IEEE Engineering in Medicine and Biology Society (EMBC)* (*25 August 2015*) (IEEE) pp 1115–8
[28] Jankelowitz S and Colebatch J 2002 Movement-related potentials associated with self-paced, cued and imagined arm movements *Exp. Brain Res.* **147** 98–107
[29] Pereira J, Ofner P, Schwarz A, Sburlea A I and Müller-Putz G R 2017 EEG neural correlates of goal-directed movement intention *Neuroimage* **149** 129–40
[30] Pereira J, Sburlea A I and Müller-Putz G R 2018 EEG patterns of self-paced movement imaginations towards externally-cued and internally-selected targets *Sci. Rep.* **8** 13394
[31] Schwarz A, Ofner P, Pereira J, Sburlea A I and Müller-Putz G R 2017 Decoding natural reach-and-grasp actions from human EEG *J. Neural. Eng.* **15** 016005
[32] Hernández-Rojas L G, Montoya O M and Antelis J M 2020 Anticipatory detection of self-paced rehabilitative movements in the same upper limb from EEG signals *IEEE Access* **8** 119728–43
[33] Ofner P, Pereira J, Schwarz A and Müller-Putz G R 2019 Online detection of hand open vs palmar grasp attempts in a person with spinal cord injury *Proc. 8th Graz Brain-Computer Interface Conf. 2019* (*September 2019*)
[34] Omedes J, Schwarz A, Montesano L and Müller-Putz G 2017 Hierarchical decoding of grasping commands from EEG *2017 39th Annual Int. Conf. IEEE Engineering in Medicine and Biology Society (EMBC)* (*11 July 2017*) (IEEE) pp 2085–8
[35] Congedo M, Barachant A and Bhatia R 2017 Riemannian geometry for EEG-based brain-computer interfaces; a primer and a review *Brain-Comput. Interfaces* **4** 155–74
[36] Guan S, Zhao K and Yang S 2019 Motor imagery EEG classification based on decision tree framework and Riemannian geometry *Comput. Intell. Neurosci.* **2019** 5627156
[37] Gaur P, McCreadie K, Pachori R B, Wang H and Prasad G 2019 Tangent space features-based transfer learning classification model for two-class motor imagery brain–computer interface *Int. J. Neural Syst.* **29** 1950025
[38] Lawhern V J, Solon A J, Waytowich N R, Gordon S M, Hung C P and Lance B J 2018 EEGNet: a compact convolutional neural network for EEG-based brain–computer interfaces *J. Neural. Eng.* **15** 056013
[39] Roy Y, Banville H, Albuquerque I, Gramfort A, Falk T H and Faubert J 2019 Deep learning-based electroencephalography analysis: a systematic review *J. Neural. Eng.* **16** 051001
[40] Mane R, Chew E, Chua K, Ang K K, Robinson N, Vinod A P, Lee S W and Guan C 2021 FBCNet: a multi-view convolutional neural network for brain-computer interface (arXiv:2104.01233)
[41] Zhang X, Xu G, Mou X, Ravi A, Li M, Wang Y and Jiang N 2019 A convolutional neural network for the detection of asynchronous steady state motion visual evoked potential *IEEE Trans. Neural. Syst. Rehabil. Eng.* **27** 1303–11
[42] Chen M, Zhang X, Chen X, Zhu M, Li G and Zhou P 2016 FastICA peel-off for ECG interference removal from surface EMG *Biomed. Eng. Online* **15** 1
[43] Solnik S, DeVita P, Rider P, Long B and Hortobágyi T 2008 Teager–Kaiser operator improves the accuracy of EMG onset detection independent of signal-to-noise ratio *Acta Bioeng. Biomech.* **10** 65
[44] Liu D, Chen W, Chavarriaga R, Pei Z and Millán J D R 2017 Decoding of self-paced lower-limb movement intention: a case study on the influence factors *Front. Hum. Neurosci.* **11** 560
[45] Sburlea A I, Montesano L and Minguez J 2015 Continuous detection of the self-initiated walking pre-movement state from EEG correlates without session-to-session recalibration *J. Neural. Eng.* **12** 036007
[46] Pfurtscheller G and Da Silva F H 1999 Event-related EEG/MEG synchronization and desynchronization: basic principles *Clin. Neurophysiol.* **110** 1842–57
[47] Gramfort A *et al* 2013 MEG and EEG data analysis with MNE-Python *Front. Neurosci.* **7** 267
[48] Yger F, Berar M and Lotte F 2016 Riemannian approaches in brain-computer interfaces: a review *IEEE Trans. Neural. Syst. Rehabil. Eng.* **25** 1753–62
[49] Minitab LLC 2021 *Minitab* (available at: https://support.minitab.com/en-us/minitab/18/help-and-how-to/modeling-statistics/anova/how-to/one-way-anova/methods-and-formulas/grouping-information-table/) (Accessed 19 March 2022)
[50] Kalunga E K, Chevallier S and Barthélemy Q Transfer learning for SSVEP-based BCI using Riemannian similarities between users *2018 26th European Signal Processing Conf. (EUSIPCO)* (*3 September 2018*) (IEEE) pp 1685–9
[51] Chevallier S, Kalunga E, Barthélemy Q and Yger F 2018 Riemannian classification for SSVEP based BCI: offline versus online implementations Brain–Computer Interfaces Handbook: Technological and Theoretical Advances (Boca Raton, FL: CRC Press)
[52] Barachant A, Bonnet S, Congedo M and Jutten C 2013 Classification of covariance matrices using a Riemannian-based kernel for BCI applications *Neurocomputing* **112** 172–8
[53] Jochumsen M, Niazi I K, Mrachacz–Kersting N, Farina D and Dremstrup K 2013 Detection and classification of movement-related cortical potentials associated with task force and speed *J. Neural. Eng.* **10** 056015
[54] Wang J, Bi L, Fei W and Guan C 2020 Decoding single-hand and both-hand movement directions from noninvasive neural signals *IEEE Trans. Biomed. Eng.* **68** 1932–40
[55] Rodríguez–Ugarte M, Iáñez E, Ortíz M and Azorín J M 2017 Personalized offline and pseudo-online BCI models to detect pedaling intent *Front. Neuroinform.* **11** 45
[56] Hasan S S, Siddiquee M R and Bai O Supervised classification of EEG signals with score threshold regulation for pseudo-online asynchronous detection of gait intention *2019 18th IEEE Int. Conf. on Machine Learning and Applications (ICMLA)* (*16 December 2019*) (IEEE) pp 1476–9
[57] Pereira J, Kobler R, Ofner P, Schwarz A and Müller–Putz G R 2021 Online detection of movement during natural and self-initiated reach-and-grasp actions from EEG signals *J. Neural. Eng.* **18** 046095